Stray Parameter Evaluation of Voltage Transformers for PQ Measurement in MV Applications

Domenico Giordano[(1)], Gabriella Crotti[(1)], Palma Sara Letizia[(1)], Daniele Palladini[(2)]

[(1)] Istituto nazionale di Ricerca Metrologica Torino, Italy
[(2)] Ricerca sul Sistema Energetico – RSE S.p.A.Milano, Italy

The work presented is developed in the project EMPIR 19NRM05 IT4PQ. This project 19NRM05 IT4PQ has received funding from the EMPIR programme co-financed by the Participating States and from the European Union's Horizon 2020 research and innovation programme.

Full Citation of the original article published: D. Giordano, G. Crotti, P. S. Letizia and D. Palladini, "Stray Parameter Evaluation of Voltage Transformers for PQ Measurement in MV Applications," 2022 20th International Conference on Harmonics & Quality of Power (ICHQP), 2022, pp. 1-6, doi: 10.1109/ICHQP53011.2022.9808555.

Available at: https://ieeexplore.ieee.org/document/9808555

Stray Parameter Evaluation of Voltage Transformers for PQ Measurement in MV Applications

Domenico Giordano
Gabriella Crotti
Palma Sara Letizia
Istituto nazionale di Ricerca Metrologica
Torino, Italy
d.giordano@inrim.it

Daniele Palladini
Ricerca sul Sistema Energetico – RSE S.p.A.
Milano, Italy
daniele.palladini@rse-web.it

***Abstract*— Power Quality (PQ) monitoring is one of the key tasks in modern power systems. In transmission and distribution grids, PQ phenomena are often measured by inductive Voltage Transformers (VTs) installed for metering and/or protection applications. VTs accuracy requirements should be ideally met under actual operating conditions, which can differ from the calibration ones, in particular for the presence of environmental or circuital influence factors. The impact of such influence factors on the VT performance in PQ measurements is an open issue, not fully addressed in the literature. In this respect, this paper presents a simplified numerical-experimental model of inductive MV VTs, which can be used for the analysis of VT wideband behaviour in PQ applications, also in presence of one or more influence factors. The results provided by the model are experimentally validated and future applications are discussed.**

***Index Terms*-- Voltage Transformer; Power quality Measurements; Influence factors; Circuital Model.**

I. INTRODUCTION

Monitoring of the quality of the electrical power in transmission as well as in distribution grids operating at Medium Voltage (MV) necessarily requires the use of measurement systems which include Instrument Transformers (ITs), to reduce the grid high voltage to levels matching the Low Voltage (LV) input of the Power Quality (PQ) measuring device. Main characteristics of the grid voltage at the user's supply terminal and limits for the PQ disturbances are issued at regional or national levels (see for example [1]). Classification and typical range of variation of disturbances are also available [2].

To ensure compliance with this limit, and more generally provide an accurate evaluation of the grid PQ conditions, the adopted measurement systems should be capable of measuring the disturbances with an uncertainty significantly lower (e.g. one order of magnitude) than the measured phenomena, considering their amplitude and frequency spectrum.

Standard [3] provide indications on measurement and test methods as well on the required measurement uncertainty relevant to PQ measuring instruments. As to instrument transformers, reference has to be made to the IEC 61968 standard series, where Voltage Transformers (VTs) accuracy classes in terms of IT ratio and phase errors are given under rated temperature and frequency conditions for the inductive VTs [4]. For the low power output voltage transformers (LPVTs) used for PQ measurement, accuracy classes and relevant limits are also given at rated temperature, as a function of frequency [5].

VTs accuracy requirements should be ideally met under actual operating conditions, which can differ from the calibration ones, as regards temperature and humidity conditions, effects of energized adjacent phases as well as proximity to grounded or floating structures, measuring circuit loading, electromagnetic interference, and mechanical vibrations. Tests to quantify the influence of such parameters on VTs and LPVTs are prescribed, but at power frequency only. As to scientific literature, it generally concentrates on the analysis of the influence of these parameters on LPIT [6]-[9].

Increasing knowledge and quantification of the possible effects of influence parameters on the VTs when measuring PQ parameters in distribution grids is one of the specific objectives of the 19NRM05 project IT4PQ [10], presently running within the European Programme for Innovation and Research (EMPIR). In this contest, the use of a validated model can facilitate the prediction of the VT performances and the evaluation of its sensitivity when measuring PQ parameters in presence of simultaneous influence factors (e.g. harmonic measurement as a function of temperature, load and presence of grounded, floating or energized structures). In the paper, the main features of a simplified VT model are presented. The model, based on a lumped parameters circuital approximation, is designed for solid insulation VTs, which are often installed in MV distribution grid applications (1 kV to 36 kV). Differently from other proposed VT models, [11]-[13], the presented one is based on a quite simple integrated numerical/experimental approach, which allows to reconstruct the VT performances from the 2nd harmonic up to the first resonance frequency. In addition, the experimental tests

conditions are chosen so that the VT core operates under rated magnetized conditions.

The paper is organized as follows: Section II presents the VT laboratory characterization procedure and the related results. In Section III the proposed circuital model is described and validated by comparison with experimental results. Finally, Section IV draws the conclusions.

II. VT Laboratory Measurement/Characterization

A. Device under test

The modeled VT is a commercial resin insulated VT for MV phase-to-ground measurement application. The VT main rated features are:

1) primary voltage 20/√3 kV;
2) secondary voltage 100/√3 V;
3) frequency 50 Hz;
4) burden 30 VA;
5) accuracy class 0.5.

B. Measurement Setup

The analyzed VT is characterized with open and short-circuit tests. Considering the VT equivalent circuit model, the open circuit test provides information on the magnetizing branch of the VT, whereas the short-circuit test allows the evaluation of the VT series parameters.
To perform the tests, two different generation and measurement setups are required as detailed in the following.

- *Open circuit*

The generation and measurement system for the open circuit test is shown in Figure 1. The MV open-circuit voltage (v_{OC}) is obtained using an Arbitrary Waveform Generator (AWG) coupled with a high voltage power amplifier. The AWG is the National Instrument (NI) PCI eXtension for Instrumentation (PXI) 5421 board (16-bit, variable output gain, ±12 V output range, 100 MHz maximum sampling rate, 256 MB onboard memory). The LV signal generated by the AWG is amplified by the high voltage power amplifier (±30 kV, ±20 mA voltage and current output capability, DC to 20 kHz bandwidth).

The applied voltage is measured by a reference resistive capacitive voltage divider (RCVD) designed, built and characterized at INRIM [14]. The RCVD rated primary voltage is ±30 kV and its frequency response is flat within 125 ppm and 350 µrad up to 9 kHz.

The primary and secondary side currents are measured by means of two Fluke A40B reference current shunts with 1/0.8 A/V and 20/0.8 mA/V transformation ratio, respectively.

The acquisition system is composed by a NI compact Data AcQuisition system (cDAQ) chassis with various boards (24-bit resolution, 50 kHz maximum sampling rate and input range from ±500 mV to ±425 V).

- *Short circuit*

The generation and measurement setup for the short-circuit measurement is shown Figure 2. The short-circuit voltage (v_{SC}) is generated by the NI AWG previously described, which is coupled with the NF HSA4011 High Speed Bipolar Amplifier (±150 V, 1 A, from DC to 1 MHz).

For the measurement of the primary side voltage no reference sensor is used, since the v_{SC} test waveform amplitude (100 V) is compatible with the input range of the acquisition system.

The primary and secondary side currents are converted into voltage by two current shunts: for the primary side the Fluke A40B reference shunt (20/0.8 mA/V) is used, whereas the secondary side device is a Tinsley Standard Resistor (4.5/2.25 A/V). The acquisition system is the one used for the open-circuit test.

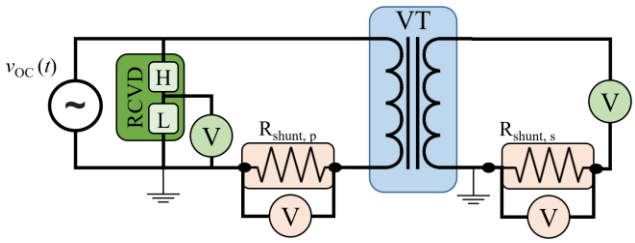

Fig. 1. Measurement setup for the VT open-circuit test

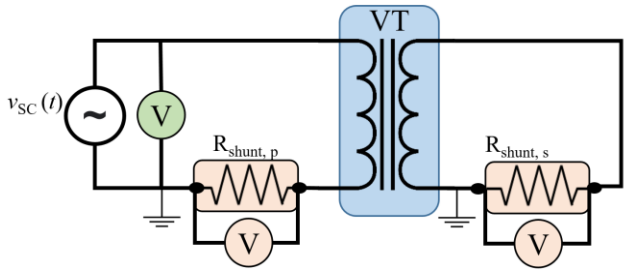

Fig. 2. Measurement setup for the VT short-circuit test

C. Test Waveforms Description

The VT is characterized with two different test waveforms: in the first case, the VT is tested with a sinusoidal waveform at rated conditions, whereas, in the second case, a voltage signal composed by a fundamental tone with one superimposed harmonic is used.

D. Sinusoidal Test

The VTs is characterized with a sinusoidal test waveform at rated amplitude and rated frequency. This test is carried out to compensate for the VT non linearity errors [15]. In fact, due to the iron-core non-linearity, if a VT is supplied with a pure sinusoidal waveform, the secondary voltage is distorted, because of the spurious harmonic components of the magnetization current [16]. This error can be reduced by preliminary measuring the spurious harmonic tones at the VT secondary side under rated sinusoidal supply. Then, the measured phasors are used as correction factors for the measurement in distorted conditions [15].

E. FH1: Fundamental Plus 1 Harmonic

The VT harmonic performances are assessed under bi-tone test waveforms, (in the following FH1, Fundamental plus one Harmonic). In particular, the FH1 waveforms are composed by a fundamental component at rated amplitude and frequency

and one harmonic tone with amplitude equal to 10 % of the rated one and harmonic order h varying from the 2nd up to 200th.

F. Measurement Results

The quantities evaluated are the VT input impedance measured when the secondary winding is open and short-circuited, respectively. Moreover, to assess the VT performance in harmonic measurement the frequency behaviors of the ratio error (1) and phase error (2) are evaluated:

$$\varepsilon_h = \frac{k_r V_{s,h} - V_{p,h}}{V_{p,h}} \quad (1)$$

$$\varphi_h = \varphi_{s,h} - \varphi_{p,h} \quad (2)$$

where:

- $k_r = \frac{V_{p,r}}{V_{s,r}}$ is the rated transformation ratio ($V_{p,r}$ and $V_{s,r}$ are the rated primary and secondary voltages);
- $V_{p,h}$ and $V_{s,h}$ are the root mean square (rms) values of the primary and secondary h-order harmonic voltage;
- $\varphi_{p,h}$ and $\varphi_{s,h}$ are the phase angles of the primary and secondary h-order harmonic voltage-

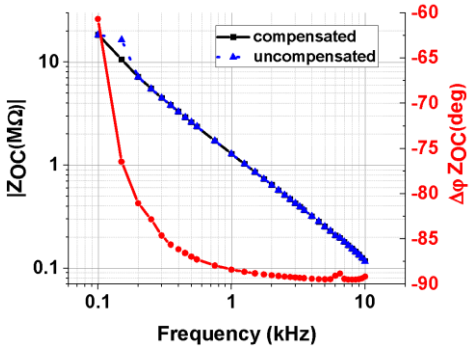

Fig. 3. VT input impedance measured in open circuit condition

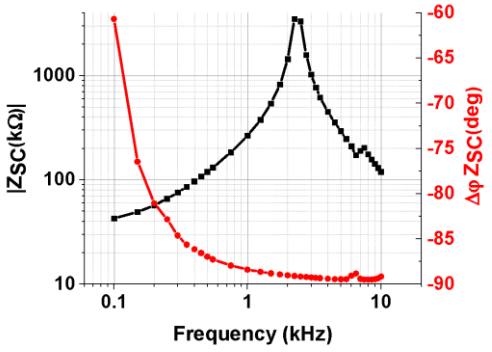

Fig. 4. VT input impedance measured in short-circuit condition

The VT input impedance in open-circuit condition $\dot{Z_{OC}}$ is shown in Figure 3. The impedance is given in terms of magnitude and phase. The magnitude response is shown before (blue line/triangle marker) and after (black line/square marker) the non-linearity compensation. As can be observed, the VT $\dot{Z_{OC}}$ shows a dominant capacitive behavior, since the magnitude impedance is inversely proportional to the \frequency f.

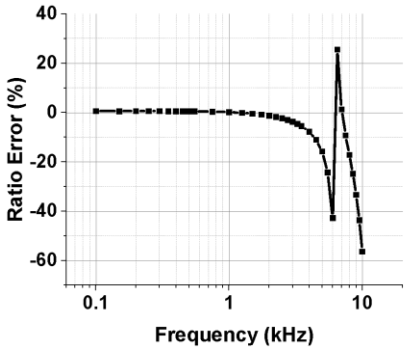

Fig. 5. VT ratio error frequency response

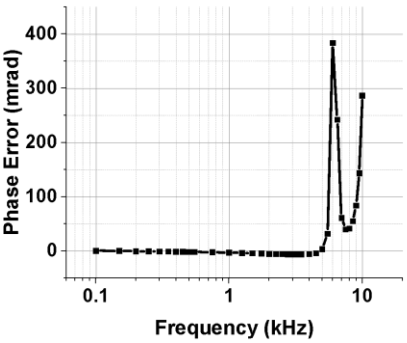

Fig. 6. VT phase error frequency response

In Figure 4 the VT input impedance in short circuit condition $\dot{Z_{SC}}$ is shown. In this case, the VT shows a resistive-inductive behavior and a first resonance at 2.3 kHz can be observed. Figure 5 and Figure 6 shows the frequency behavior of the ratio and phase errors respectively. As can be observe the analyzed VT has a quite flat response for the first harmonics and the first resonance is at 6 kHz.

III. Circuital Model

Several circuital model for the frequency analysis of the behavior of power transformer can be found in literature. The most common model that takes into account the stray capacitances among the active elements of the transformers is provided e.g. in [17]. Following this approach, the authors adopt the model shown in Figure 7.

The stray couplings between the primary winding and ground, the secondary winding and ground, and the primary and secondary winding are represented by C_H, C_L and $C_{H\text{-}L}$ respectively. Such quantities are frequency independent.

The inductive coupling is described by the typical model of two windings magnetically coupled, whose characterizing parameters are the primary and secondary auto-inductance L_1 and L_2 and the coupling coefficient k which is defined as:

$$k = \frac{M}{\sqrt{L_1 \cdot L_2}} \tag{3}$$

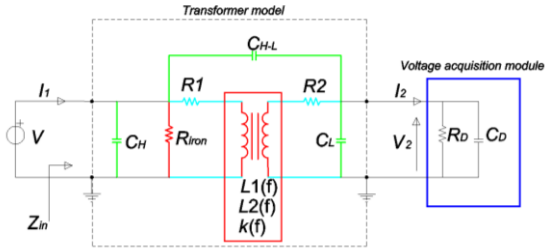

Fig. 7. VT circuital model of the VT

where M is the mutual coupling between the windings. It is important to highlight that, because of the frequency dependence of the induction inside the iron core, all these quantities depend on the signal frequency. The induction in the iron core decreases with the frequency for two main reasons: the eddy currents and the frequency behavior of the iron relative permeability. They affect both the mutual and leakage inductance and consequently the VT resonance. The VT model is completed by the resistance of the two windings R1 and R2.

In the following, the procedure to quantify the model parameters is provided.

A. *Stray capacitance determination*

The first step is the determination of the stray electrical coupling between the active elements of the VT. To this end three elements are identified: the external surface of the primary and secondary windings and all surfaces inclosing the masses ground connected, that is the iron core and the VT metallic base. The stray capacitances are determined by solving two electrostatic problems by means of a 2D FEM (Finite Element Method) solver. In the first case a fixed voltage of 1 V is applied to the primary winding surface, while all the other masses are fixed to zero potential.

The solution of this problem provides C_H corresponding to the electric charge induced on the ground masses and $C_{H\text{-}L}$ is numerically equal to the electric charge induced on the secondary winding surface. 1 V is then applied to the secondary winding and zero to the other masses, providing the stray coupling C_L. The geometric configuration of the 2D model of the VT is given in Figure 8 (transverse section of the VT).

The relative electric permittivities of the insulation materials are 3.5, for the insulation between the windings, and 4 for the resin. The FEM problems are solved by the open software FEMM 4.2. Considering the insulation thickness between primary and secondary windings, the computed capacitance between the two windings, $C_{H\text{-}L}$ ranges between 52 pF and 75 pF; the stray capacitances C_H and C_L are found equal to 20 pF and 400 pF respectively.

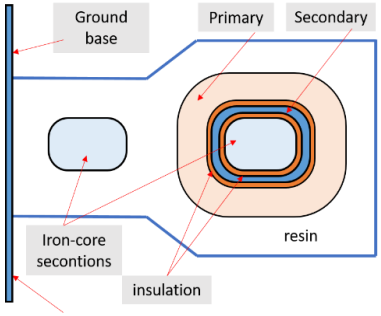

Fig. 8. 2D Geometrical configuration of the Electrostatic FEM model of the VT under test.

B. *Iron losses determination*

The losses due to the eddy currents and the iron losses are represented by resistance R_{iron}. Neglecting the power losses provided by the copper resistance of the two windings we can compute such resistance with the formula:

$$R_{iron} = \frac{V}{I_1 \cdot \cos(\varphi)} \tag{4}$$

Where V is the voltage applied to the primary, I_1 is the current measured at the input of the transformer when the secondary is in the open-circuit condition and $\cos(\varphi)$ is the power factor. Thanks to the open-circuit measurement it is possible to determine R_{iron} as a function of the applied harmonic frequency (Table 1.)

TABLE I. FREQUENCY BEHAVIOR OF R_{iron}

Frequency(Hz)	R_{iron} (MΩ)
100	39.6
200	45.9
400	48.3
1000	42.2
2000	29.5
6000	6.7
10000	2.9

C. *Inductance parameters*

The auto-inductances of the two windings, L_1 and L_2, and the winding coupling coefficient, k, are computed by exploiting the magnetic module of the 2D FEMM solver. Figure 3 provides a sketch of the geometry adopted for the inductance coupling determination. The simulation has been performed by selecting a linear B-H curve and is performed at different supply frequency. It is important to highlight that the FEMM simulator takes into account the eddy current effects, but not the reduction of the relative permeability, as occurs in reality.

The primary auto-inductance obtained at 100 Hz is 140 kH. Such value reduces to about 27 kH at 2 kHz and to 13 kH at 10 kHz.

The leakage inductance can be computed, at low frequency, by applying the formula:

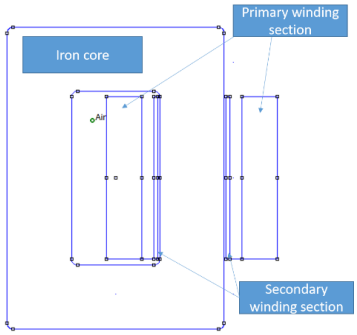

Fig. 9. Sketch of the geometry simulated for the computation of the VT inductive coupling

$$L_{leak} = \frac{2 \cdot W}{I_{mag}^2} \quad (5)$$

where W is the energy stored in the air surrounding the windings when the two windings provide the same magneto-motive force in the opposite way and I_{mag} is the magnetizing current. Such result has to be corrected because of the errors introduced by the 2D FEM approach. The corrected formula is provided by:

$$L_{leak-c} = \frac{L_{leak}}{d} \cdot 2\pi \cdot r_w \quad (6)$$

where d is the depth of the 2D FEM model and r_w is the average radius of the two windings. For the considered case, the quantity L_{leak-c} is of about 25.7 H. This quantity summarizes the leakage inductance of primary and secondary seen at primary winding. The coupling between the two windings is then evaluated by the expression:

$$k = 1 - \frac{L_{leak-c}}{L_1} \quad (7)$$

that provides a coupling coefficient k of 0.9996.

It is important to highlight that this quantity changes with the increase of the frequency. The leakage inductance depends on the geometrical configuration of the windings with respect to the iron-core. At the increase of the frequency, the stray capacitances among the turns produce a rearrangement of the current into the turns [18]. This phenomenon can be represented, in an approximated way, as a geometrical variation of the windings with a consequent dependence of the leakage inductance L_{leak} on frequency. As described in the following sub-section, this dependence is determined by performing a fit to measurement data.

D. Model performances

A first measurement-model comparison is performed for the input current at 100 Hz. The computed current is about 65 μA, while the measured one is 63 μA. Figure 10 instead provides a comparison between the computed and measurement input impedance for both magnitude and phase.

For what concern the short-circuit test, the input impedance shows a parallel resonance at about 2.3 kHz. Responsible for this resonance are mainly the leakage inductance L_{leak}, C_{H-L} and C_H. The leakage inductance L_{leak}, because of the primary intern-turn capacitances increases with frequency.

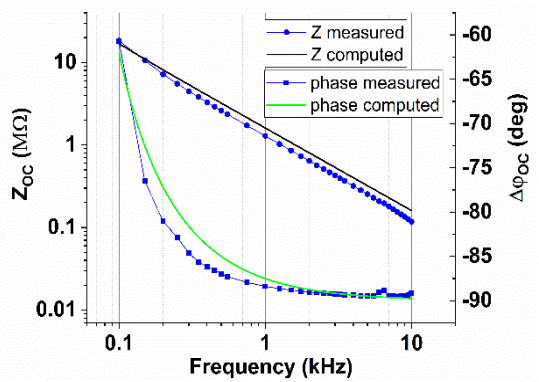

Fig. 10. Comparisons between measured (blue line – circle/triangle) and computed (Black/green line) impedances

Its amplitude behavior, at low frequency (up to 2300 Hz), is obtained by carrying out a fit that provides a good overlap between the short-circuit measurements and model data. For frequencies higher than 2300 Hz, the open-circuit measurements have been exploited to identify the leakage inductance value providing overlap with the measured ratio error. The leakage inductance behavior is summarized in Table 2.

TABLE II. SUMMARY OF LLEAK VERSUS FREQUENCY

Frequency (Hz)	L_{leak}
100	26 H
300	34 H
1000	36 H
2300	48.6 H
6000	1200 H

The value of L_{leak} at 100 Hz proves the good agreement between the leakage inductance computed by the 2D FEMM program (25.7 H). A frequency sweeps of the input impedance computed for different value of L_{leak} is shown in Figure 11. The same figure also shows the measured impedance and the impedance computed at 100 Hz, 300 Hz, 1 kHz, 2.3 kHz and 6 kHz (yellow circles), assuming, for each frequency, the leakage inductance value provided in Table 2. The comparison between the measured and computed ratio error, at high frequency, for the open-circuit test is provided in Figure 12.

A preliminary analysis of the impact of stray capacitances variation has been carried out. With this simplified model, the stray capacitive coupling responsible for the resonance frequency variation is the one between primary and secondary windings (C_{H-L}). Table 3 summarizes the resonance frequencies as a function of the stray capacitance C_{H-L} value.

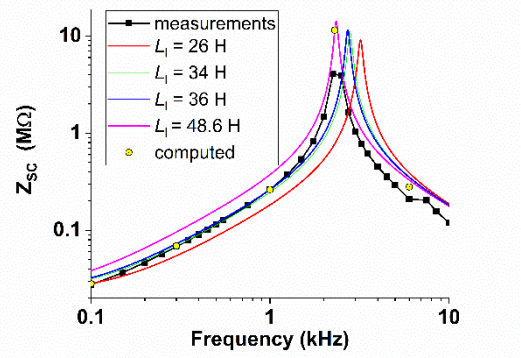

Fig. 11. Comparison between measured and computed input impedance in short-circuit conditions with constant and changing leakage inductance with frequency.

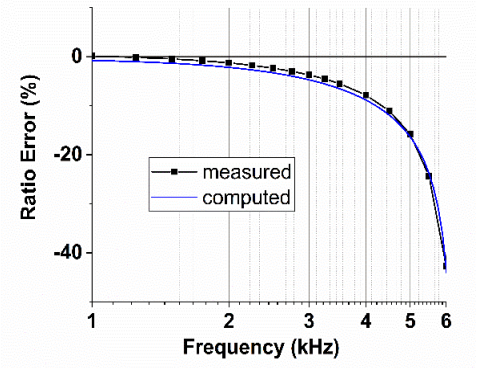

Fig. 12. Comparison between measured and computed VT ratio error.

TABLE III. CH-L EFFECT ON THE RESONANCE FREQUENCY

$C_{H\text{-}L}$ (pF)	f_{res} (kHz)
50 pF	8
75 pF	6.6
100 pF	5.7

RESULTS DISCUSSION AND CONCLUSIONS

The VT simplified model has been developed by making use of an integrated numerical-experimental approach. The electrical stray parameters of the VT equivalent circuit are obtained from a simplified 2D geometrical representation, whereas the VT inductive parameters are worked out starting from available magnetic core data. Additional input data and model refinement are provided by experimental measurements. Validation has been performed by comparison with open-circuit and short-circuit frequency sweeps, which are carried out supplying the magnetic core with a fundamental tone plus one harmonic tone. The comparison of the VT model output quantities with the corresponding measured ones (primary current and input impedances, measured ratio and phase errors) shows an agreement within some percent up to several kilohertz.

Activity will now be focused on the performance of the VT model, when used to predict effects on measured PQ parameters due to the presence of one or more influence parameters (such as temperature variation and grounded structure, ecc), which can be determined starting from the variation of the VT model stray parameters.

ACKNOWLEDGMENT

The work here presented has been developed within the EMPIR 19NRM05 IT4PQ project, which has received funding from the EMPIR programme co-financed by the Participating States and from the European Union's Horizon 2020 research and innovation programme.

REFERENCES

[1] Voltage characteristics of electricity supplied by public electricity networks, EN 50160, 2010.
[2] *IEEE Recommended Practice for Monitoring Electric Power Quality, IEEE 1159-2019.*
[3] IEC 61000-4-30 Electromagnetic compatibility (EMC) - Part 4-30: Testing and measurement techniques - Power quality measurement methods, IEC, 2015
[4] IEC 61869-3 Instrument transformers - Part 3: Additional requirements for inductive voltage transformer, IEC, 2011
[5] IEC 61869-6 Instrument transformers - Part 6: Additional general requirements for low-power instrument transformers, IEC 2016
[6] Hrbac, R., Kolar, V., Bartlomiejczyk, M., Mlcak, T., Orsag, P., & Vanc, J. (2020). "A Development of a Capacitive Voltage Divider for High Voltage Measurement as Part of a Combined Current and Voltage," Sensor. Elektronika Ir Elektrotechnika, 26(4), 25-31.
[7] Mingotti, A.; Costa, F.; Peretto, L.; Tinarelli, R. "Effect of Proximity, Burden, and Position on the Power Quality Accuracy Performance of Rogowski Coils," Sensors 2022, 22, 397. https://doi.org/10.3390/s22010397
[8] Mingotti A, Costa F, Pasini G, Peretto L, Tinarelli R. "Modeling Capacitive Low-Power Voltage Transformer Behavior over Temperature and Frequency," Sensors. 2021; 21(5):1719.
[9] C. Gonzalez, S. Weckx, T. De Rybel and J. Driesen, "Dynamic Thermal Modeling of Voltage Divider Capacitive Coupling," in IEEE Transactions on Power Delivery, vol. 31, no. 3, pp. 1015-1025, June 2016, doi: 10.1109/TPWRD.2015.2392386.
[10] https://www.it4pq.eu/
[11] F. D. Torre et al., "Instrument transformers: A different approach to their modeling," 2011 IEEE International Workshop on Applied Measurements for Power Systems (AMPS), 2011, pp. 37-42, doi: 10.1109/AMPS.2011.6090433.
[12] C. Buchhagen, et al., "Calculation of the frequency response of inductive medium voltage transformers," 2012 IEEE International Energy Conference and Exhibition (ENERGYCON), 2012, pp. 794-799, doi: 10.1109/EnergyCon.2012.6348259.
[13] M. Kaczmarek and E. Stano, "Nonlinearity of Magnetic Core in Evaluation of Current and Phase Errors of Transformation of Higher Harmonics of Distorted Current by Inductive Current Transformers," in IEEE Access, vol. 8, pp. 118885-118898, 2020, doi: 10.1109/ACCESS.2020.3005331.
[14] G. Crotti *et al.*, "Frequency Compliance of MV Voltage Sensors for Smart Grid Application," in IEEE Sensors Journal, vol.17, no.23, 2019.
[15] A. Cataliotti *et al.*, "Compensation of Nonlinearity of Voltage and Current Instrument Transformers," *IEEE Transactions on Instrumentation and Measurement*, vol. 68, n. 5, May. 2019
[16] G. Crotti, G. D'Avanzo, P. S. Letizia and M. Luiso, "Measuring Harmonics with Inductive Voltage Transformers in Presence of Subharmonics," in IEEE Transactions on Instrumentation and Measurement, vol. 70, pp. 1-13, 2021, Art no. 9005013,
[17] S. Zhao, et al., "Testing and modelling of voltage transformer for high order harmonic measurement," 2011 4th International Conference on Electric Utility Deregulation and Restructuring and Power Technologies (DRPT), 2011, pp. 229-233.
[18] M. Chiampi, G. Crotti and D. Giordano, "Set Up and Characterization of a System for the Generation of Reference Magnetic Fields From 1 to 100 kHz," in IEEE Transactions on Instrumentation and Measurement, vol. 56, no. 2, pp. 300-304, April 2007, doi: 10.1109/TIM.2007.890611.